Exchange Geometry Revealed by Float Trajectories in the Gulf Stream*

M. SUSAN LOZIER

Duke University, Durham, North Carolina

LAWRENCE J. PRATT AND AUDREY M. ROGERSON

Woods Hole Oceanographic Institution, Woods Hole, Massachusetts

P. D. MILLER

Center for Fluid Mechanics, Brown University, Providence, Rhode Island

(Manuscript received 24 June 1996, in final form 21 January 1997)

ABSTRACT

In an effort to understand the extent to which Lagrangian pathways in the Gulf Stream indicate fluid exchange between the stream and its surroundings, trajectories of RAFOS floats are viewed in a frame of reference moving with the dominant zonal phase speed associated with the periodic flow. In such a frame, geometrical structures emerge that more clearly delineate the position of the parcel in relation to the jet core and its surroundings. The basic premise of this work is that the pathways of fluid parcels in the vicinity of stagnation points, as defined in the moving frame of reference, are susceptible to changes in their pathways, thereby facilitating fluid exchange between different regions of the flow field. Four representative RAFOS float trajectories are shown to exhibit the expected behavior in the vicinity of stagnation points. To further examine the mechanism of exchange in the vicinity of these geometrical features, concepts from dynamical systems theory are applied to a numerically simulated flow field. The entrainment and detrainment of parcels from the jet core are explained in the context of stable and unstable manifolds and their associated lobes. It is shown that the Lagrangian pathways from the numerical flow and the observational trajectories exhibit a similarity based on the kinematics of a meandering flow field. Overall, this study provides the first look at RAFOS float trajectories in a moving frame and provides insight as to how the temporal variability of a jet creates chaotic exchange.

1. Introduction

Over the past two decades SOFAR and RAFOS floats have been used extensively to map current paths and to infer characteristics of mixing along those paths. Interpretations of these float trajectories, in the Gulf Stream and elsewhere, have been aided in the past five years by a number of simple models that were developed for the study of Lagrangian motion in meandering jets (Bower 1991; Pierrehumbert 1991; Behringer et al. 1991; Samelson 1992; Lozier and Bercovici 1992; Dutkiewicz et al. 1993; del-Castillo-Negrete and Morrison 1993; Meyers 1994; Pratt et al. 1995; Duan and Wiggins; 1996). An idea central to most of these studies is

that the interpretation of Lagrangian motion is greatly simplified when the flow field is viewed in a frame of reference moving with the phase speed of the periodic flow. As will be discussed in the next section, in such a frame underlying geometrical structures emerge that more clearly delineate a parcel's position relative to the jet and its surroundings.

Because float data have not traditionally been accompanied by contemporaneous phase speed data, observational trajectories have not generally been viewed in a moving frame of reference. Recently, however, Lee (1994) (see also Lee and Cornillon 1996a,b) has calculated Gulf Stream meander phase speeds using AVHRR images for the period April 1982 through December 1989, encompassing the period during which RAFOS floats were seeded in the Gulf Stream. By matching Lee's phase speeds to the RAFOS float data it has been possible to view a small number of trajectories in appropriate moving-frame coordinates. In this paper we describe these moving-frame trajectories and interpret their structure and evolution in terms of the meandering flow field. To aid our interpretation we compare the RAFOS float trajectories to results from a nu-

Corresponding author address: Dr. M. Susan Lozier, Division of Earth and Ocean Sciences, Nicholas School of the Environment, Duke University, Old Chemistry Building, Box 90227, Durham, NC 27708-0227.
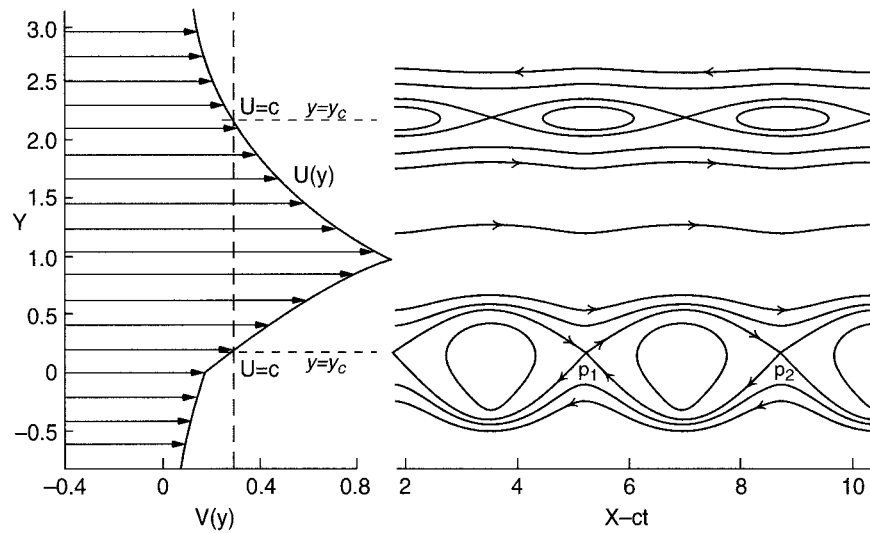E-mail: s.lozier@duke.edu

FIG. 1. Moving-frame trajectories (right-hand side) in an asymmetric jet (left-hand side). The critical lines are marked by the lines, $y = y_c$. The symbols p_1 and p_2 designate stagnation points. Arrows are used to indicate flow direction. (From Pratt et al. 1995.)

merical model, for which a dynamical systems analysis is used to facilitate the description of Lagrangian motion (Rogerson et al. 1997). The overall purpose of this work is to illustrate how the use of a moving frame of reference for Gulf Stream trajectories can further our understanding of Lagrangian pathways. Specifically, we are interested in how this frame of reference contributes to our understanding of cross-frontal exchange processes.

In the next section, a brief summary of the idealized flow geometry in a moving frame of reference is given. In section 3 the data and methods are discussed, followed by a description of the RAFOS float trajectories in section 4. In section 5 mechanisms of exchange are discussed, followed by numerical model results in section 6 and a summary in section 7.

2. Moving-frame geometry

As an introduction to the geometric framework that is the focus of this study, consider a jet flowing in the x direction (eastward) with velocity $U(y)$, as depicted in the left-hand portion of Fig. 1. This velocity profile is based on the equivalent barotropic model discussed by Pratt et al. (1995), but its form is generally unimportant in what follows. A meandering jet can be formed from a parallel basic flow, $U(y)$, by adding a linear normal mode of the form

$$\phi(x, y, t) = \Phi(y) \cos k(x - ct), \quad (1)$$

where ϕ is the perturbation streamfunction and k and c are the wavenumber and phase speed of the meander, respectively. The right-hand portion of Fig. 1 shows streamlines for the flow field obtained by adding one such mode to the basic jet and viewing the results in a

frame of reference moving with the (positive) meander phase speed, c. Because the disturbance is neutrally stable (k and c are real), the flow appears steady in the moving frame of reference. Thus, in this frame the streamlines shown in Fig. 1 also define the pathways of fluid particles. The most notable feature formed by the streamlines are two rows of cat's eyes, one on each side of the asymmetric jet. The cat's eyes are centered at the critical (or steering) lines, $y = y_c$, of the basic flow, defined by $U(y_c) = c$, and are bounded by a set of streamlines that intersect at the fixed (or stagnation) points that appear in the moving frame. In dynamical systems theory, these bounding streamlines are referred to as stable and unstable manifolds of the fixed points. For example, the curve leading away from the fixed point p_1 in the northeast direction is an unstable manifold of p_1, whereas the curve approaching p_1 from the southeast is a stable manifold of p_1. The latter is also an unstable manifold of the fixed point p_2, while the former is a stable manifold of p_2. Note that these structures would be lost in stationary-frame plots of fluid motion. Also of note in Fig. 1 is that the amplitude (meridional extent) of the cat's eyes can be much larger than the amplitude of the meandering of the jet axis. As discussed by Pratt et al. (1995), this implies that parcel exchange can possibly occur over a meridional extent larger than the jet's streamline displacements.

Because the manifolds separate "open" and "closed" streamlines, fluid pathways in the vicinity of these manifolds are quite sensitive to small amounts of diffusion, noise, or any other influence that would cause a departure from the paths shown in Fig. 1. If a parcel were to occasionally cross a manifold, it would alternately move along a path either outside or inside of the cat's eyes. Such a pathway would considerably facilitate fluid ex-
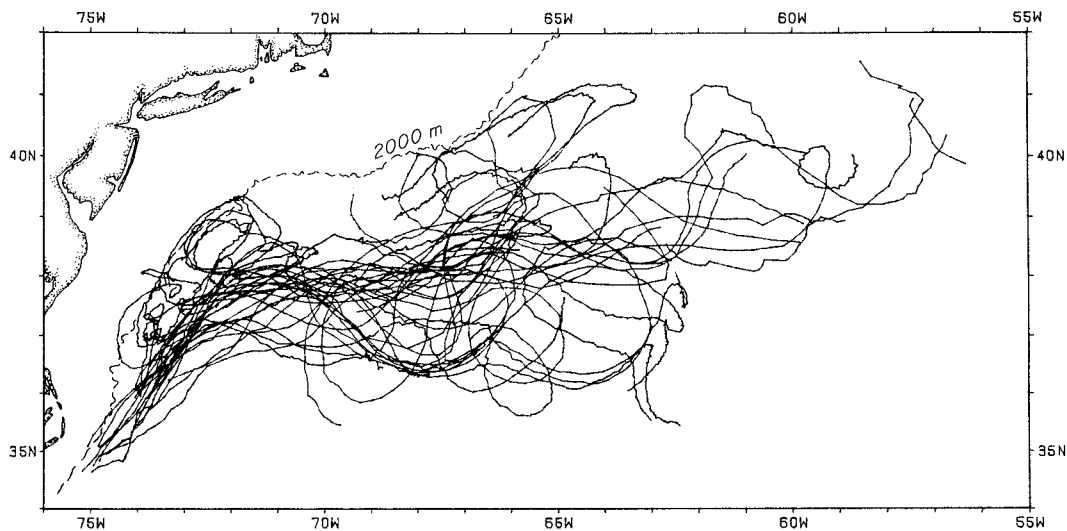
FIG. 2. Composite of RAFOS floats launched sequentially in the Gulf Stream at thermocline depths. (From Bower and Rossby 1989.)

change. Many of the studies cited in section 1 explore ways of perturbing the trajectories so as to induce this exchange, and hence mixing, in the vicinity of the cat's eyes. Perturbations include the introduction of a second meander, periodic pulsation of the amplitude of the primary meander, or weak diffusion. The net result of any of these secondary perturbations is chaotic motion in the vicinity of a cat's eye, as will be explored in sections 5 and 6.

In sum, in a frame of reference moving with the phase speed of the jet's dominant meander, one should expect to see evidence of critical lines, stagnation points, and cat's eyes. Given the ubiquity of secondary perturbations, it is expected that in the vicinity of these features a float is likely to experience an observable change in the character of its trajectory. For example, a float could move from a closed or open streamline region (or vice versa) in the vicinity of the cat's eye. Given this expected mixing geometry, we will examine the observational floats in the next section.

3. Data and methods: RAFOS float trajectories

Trajectories of floats and drifters have traditionally been viewed in a stationary frame where their geographic positions are plotted on a (longitude x, latitude y) grid. In a frame moving with a single wave traveling in the x direction, the positions of the float are given by the coordinates $(x - c_x t, y)$, where c_x is the phase speed of the disturbance. For the case of a float moving downstream in the Gulf Stream the phase speed is generally not constant along its path, as explained by Lozier et al. (1996). The meander can either accelerate or decelerate while the float is traveling through, or the float can move from one meander to another meander propagating at a different speed. For this reason the appro-

priate moving-frame coordinates become $(x - \int c_x(t)\, dt, y)$, where the integrated distance the meander has moved is subtracted from the total distance the float has moved. Here $c_x(t)$ represents a phase speed that changes with time since the float encounters different phase speeds along its path.

The float data used in this study were obtained as part of the RAFOS Pilot Program (Bower et al. 1986), conducted over the years 1984–85. Thirty-seven isopycnal RAFOS floats were launched sequentially in the main thermocline of the Gulf Stream off Cape Hatteras and tracked acoustically downstream for 30 or 45 days (Fig. 2). The data processed from these floats generated the geographical position, pressure, and temperature along the path of each float at an interval of 8 hours. Horizontal velocities were obtained from the time rate of change of position over 16 hours using a simple centered difference.

To obtain phase speed information during the time of the float deployments, we have relied on the analysis of Lee and Cornillon (1995; 1996a,b), who used infrared images of the sea surface temperature from the AVHRR (Advanced Very High Resolution Radiometer) to digitize the Gulf Stream path for the period of April 1982 to December 1989. They chose a rectangular grid from 22° to 48°N and 76° to 45°W that covers the full latitudinal range of the Gulf Stream from its separation near Cape Hatteras to its bifurcation near the Tail of the Grand Banks. Composites were made every 2 days with a spatial resolution of 1 km. Using a method described by Cornillon et al. (1994) the location, wavelength, and amplitude of individual meanders were objectively determined from these composites. Both meridional and zonal phase speeds (c_y and c_x, respectively) for individual meanders were then calculated by the change in meander location from one observation to the next (i.e.,
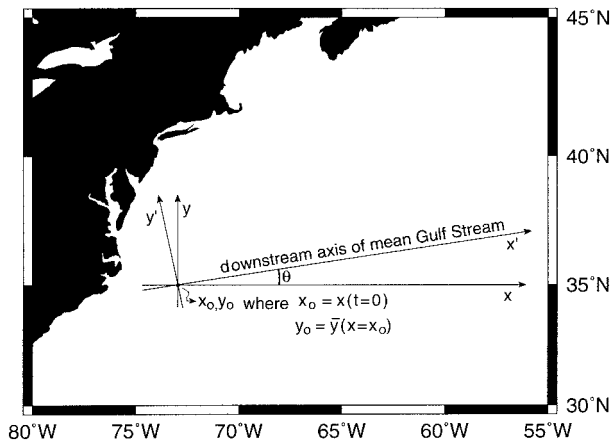
FIG. 3. Coordinate system used in the determination of RAFOS float trajectory positions. All RAFOS float trajectories shown are aligned with the downstream axis of the Gulf Stream.

over a 2-day period). Based on an rms uncertainty in the digitization of the satellite imagery of 4.8 km (Gangopadhyay 1990), the uncertainty in the phase speed measurements is approximated to be 6.7 km day^{-1}. Further details of the dataset are contained in Lee (1994).

In order to view RAFOS float trajectories in a moving frame an appropriate meander phase speed is needed. Because the Gulf Stream at any time is characterized by a number of meanders that move at different speeds (Lee 1994), it is important that there is a spatial as well as a temporal match between a float's position and a meander. To achieve this objective the location of a float was superposed on a digitized path of the Gulf Stream (from NOAA/NESDIS charts of sea surface temperature) that was also marked with the positions of the meander observations that occurred within a half-day of the float observations. The match between float and phase observation was then subjectively determined based on a visual assessment of float position and meander location. If a meander could not be identified or if there was ambiguity regarding two or more meanders, no phase speed was linked to the float observation (Lozier et al. 1996).

Once a phase speed had been identified for each float position, the moving-frame coordinates were computed for each float trajectory. An orthogonal coordinate system was chosen such that the x axis is aligned alongstream and the y axis is aligned cross-stream. These axes were chosen for each float individually based on the mean position of the Gulf Stream (as determined by satellite imagery) for the time covered by the float record. The float's alongstream and cross-stream coordinates are their distance from x_0 and y_0, where x_0 is the float's initial longitudinal position and y_0 is the mean latitudinal position for the stream at x_0. These distances were transformed onto the (x', y') axes with the (x_0, y_0) point being the mutual intersection of the two coordinate systems, as shown in Fig. 3. In the (x', y') plots, y'

represents the distance from the mean alongstream axis while x' represents the distance from the initial x' value (x_0). The float's moving frame coordinates are $(x' - c_{x'}t, y')$, with the same initial positions as the stationary frame plots.

Because phase observations were made every 2 days and float observations were made every 8 hours, we chose to smooth the float velocities with a boxcar filter of 2 days, reflecting the scale over which phase observations were made. Sensitivity studies with this smoothing scale did not significantly change our results. To compute the integral for the moving frame coordinates, c_x and c_y were transformed onto the along- and cross-stream axes so that the integral was computed using $c_{x'}$. The integral was computed discretely with dt set at 8 h, the time between float observations.

4. Observational trajectories in moving frame

Of the 37 RAFOS floats launched as part of the Pilot Program, only 8 floats have sufficient float and phase data for this study. This small recovery is primarily due to gaps created in the phase data by cloud cover, but also due to gaps in float data. Some float records were too short to be used and some floats had little or no tracking information. Of these eight float trajectories, three have a large gap of missing phase data in their total record. In these cases the phase and float data before and after the gap were considered to be separate records, bringing the total number of trajectories analyzed in the moving frame to 11. The first and second parts of the record are designated with an "a" and "b" respectively. Four of these trajectories, which cover the range of trajectory geometry, will be discussed in this section: RAFOS floats 037, 035b, 034b, and 024. It is noted here that during the transit of each of these floats there were no local ring formations or ring/stream interactions. With such events the applicability of a moving-frame system would need to be reexamined.

Each float trajectory is plotted in both the stationary and moving frame. The size of the symbol used to denote a position on the trajectory plots is proportional to the magnitude of $u' - c_{x'}$. The smallest symbol is used to denote $|u' - c_{x'}| = 0$, while the largest symbol is used to denote the maximum value of $|u' - c_{x'}|$ for that particular trajectory. When viewing the trajectories, the reader is reminded that, where the symbols are small, the float is in the vicinity of a critical line. Accompanying these trajectory plots is the Lagrangian time series for $c_{x'}$ and u'. The symbol size for the time series of u' is proportional to the pressure measured along the float's track. The symbol range spans from the minimum to the maximum pressure for that float for the portion of the record shown. Large symbols denote that the float is on the southern (or anticyclonic) side of the Gulf Stream, while small symbols denote the float is on the northern (or cyclonic) side of the stream. The symbol size for $c_{x'}$ is constant.
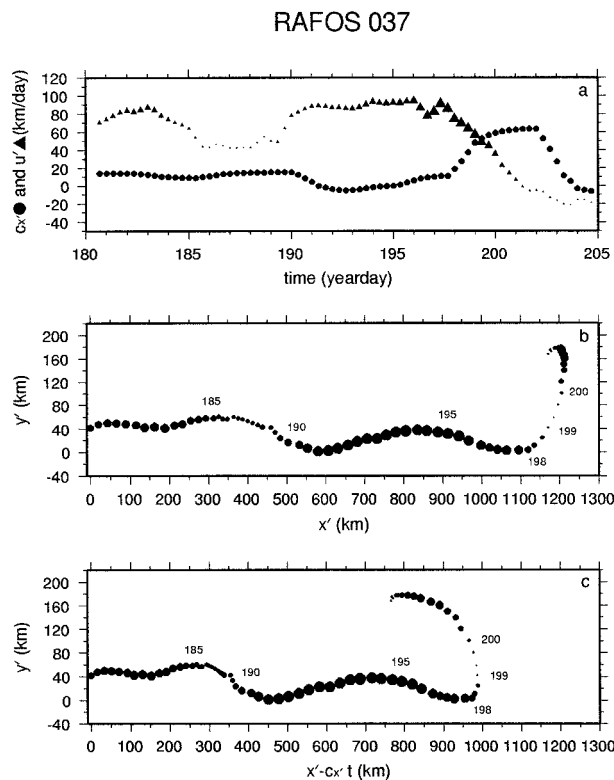
RAFOS 037

FIG. 4. RAFOS 037. (a) Time series of u' and $c_{x'}$ for the portion of the float's life with phase speed coverage. The size of the symbol for u' is proportional to the pressure along the float's path. Small values denote small pressures (onshore side of the stream) and large values denote large values (offshore side of the stream). (b) Stationary frame trajectory with symbol size proportional to $|u' - c_{x'}|$. (c) Moving-frame trajectory with symbol size proportional to $|u' - c_{x'}|$. Symbol spacing in all panels, and subsequent RAFOS trajectory plots, is 8 h.

a. RAFOS 037: Figures 4, 5, and 6

The RAFOS 037 trajectory in the moving frame differs little from the trajectory in the stationary frame for days 181 to ~198, as expected, since over that period $u' > c_{x'}$ (Fig. 4a). Near day 198 there is a sharp increase in the meander phase speed, with a zonal phase speed of ~60 cm s^{-1} reached by day 200. [Note: Although phase speeds in the Gulf Stream are typically on the order of 15–20 cm s^{-1} (Lee 1994), much larger phase speeds are also observed. Of the 2976 phase speed observations in Lee's database, 49 were larger than 40 cm s^{-1}, 13 larger than 50 cm s^{-1}, and 6 larger than 60 cm s^{-1}.] When the meander phase speed increases, the float rapidly approaches and then crosses a critical line, as seen in the time series of u' and $c_{x'}$ (Fig. 4a). At this point there is a dramatic change in the course of the trajectory, reflected in both the moving and stationary frames (Figs. 4b,c). Small amplitude progressive motion is replaced by a large amplitude displacement across the stream, as evidenced by the swift decrease in pressure as the float moves to the northern side of the stream.
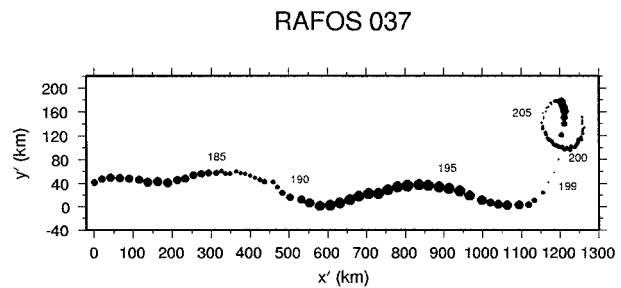
RAFOS 037

FIG. 5. Stationary frame trajectory for RAFOS 037. The path is extended over that shown in Fig. 4 to include the float days that do not have corresponding phase speed data.

Beginning near day 198 in the moving frame, it appears as though the float is tracing a cat's eye, similar to what is seen in Fig. 1. At the critical line this float has moved to an entirely different path, having been carried a large distance meridionally from its original path. Our interpretation of this trajectory is that it has traveled away from the jet core, into a cat's eye structure. An examination of RAFOS 037's path after day 205 (Fig. 5), when phase speed coverage ends, shows that the float moves back toward the stream and again moves downstream, as would be predicted for a parcel embedded within a cat's eye structure. In section 6 we show that this looping geometry in the stationary frame corresponds to the cat's eye geometry in the moving frame.

Song et al. (1995) have described the edge of the Gulf Stream by a minimum eastward velocity (chosen as 20 cm s^{-1}). With such a definition it is clear that RAFOS 037, with a zonal velocity of 60 cm s^{-1}, is not near the edge of the stream when it changes course and is apparently detrained from the jet core. To emphasize this point, the stationary and moving-frame trajectories for
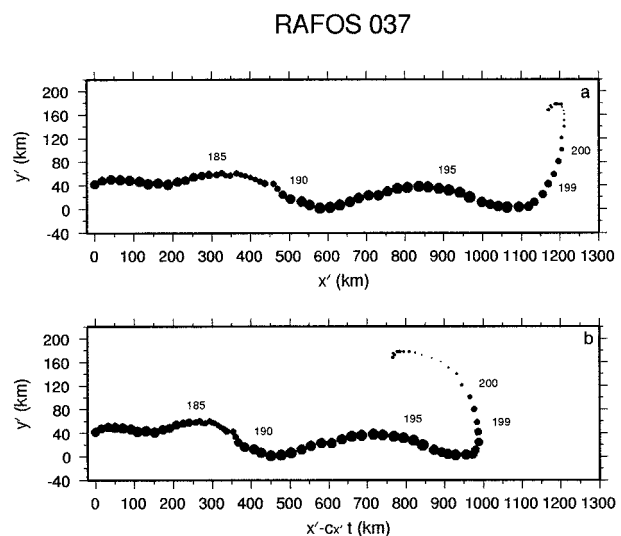
RAFOS 037

FIG. 6. RAFOS 037. (a) Stationary frame trajectory with symbol size proportional to $|u'|$. (b) Moving frame trajectory with symbol size proportional to $|u'|$.
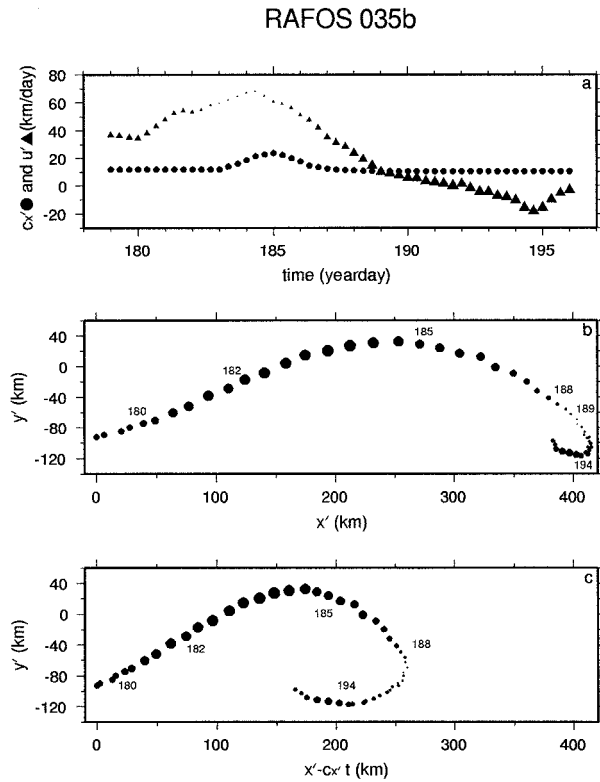
RAFOS 035b

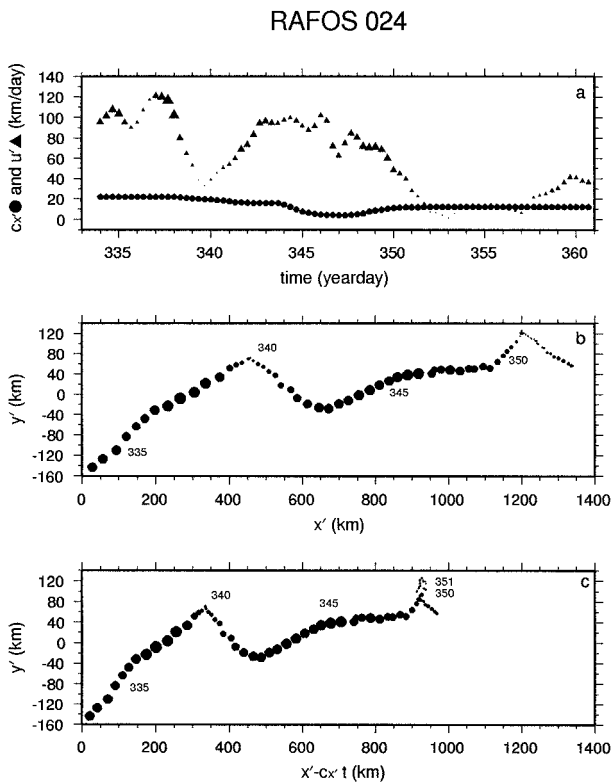FIG. 7. As for Fig. 4 but for RAFOS 035b.

RAFOS 024

FIG. 8. As for Fig. 4 but for RAFOS 024.

this float are replotted in Fig. 6, but now the symbol for each data point is proportional in magnitude to $|u'|$. It is evident that the change in path for this float occurs well before its zonal velocity diminishes, that is, well before it is near the edge of the stream, as defined by an isotach. This "premature" detrainment can be explained by the fact that the float encounters a critical line when its zonal velocity is approximately 60 cm s^{-1}, placing it between the center of the stream and its edge. It is expected that critical lines would normally lie near the edge of the stream for the depth range covered by these floats since, as mentioned above, Gulf Stream phase speeds are typically closer to 15 or 20 cm s^{-1}. In this case, however, with the critical line closer to the jet core it becomes apparent that the detrainment of this parcel is entirely due to the kinematics of the meandering jet rather than by processes at the edge of the jet, as previously discussed by Bower (1991) in the context of recirculating cells in a moving frame. Finally, while we may define the edge of the stream in the stationary frame in terms of where the eastward velocity significantly diminishes, in the moving frame it is clear that entrainment and detrainment of parcels from the jet core occurs in the vicinity of critical lines, which do not necessarily correspond with isotachs at the edge of the stream.

b. RAFOS 035b: Figure 7

The pattern of RAFOS 035b float is similar to the pattern described for RAFOS 037. The value of $u' - c_{x'}$ remains large until day 188 when the float approaches and then crosses a critical line (Fig. 7a). After it crosses the line, the float appears to be on a new path, tracing a cat's eye (Fig. 7c). The pattern of the cat's eye in this case is particularly clear. The points where $u' - c_{x'} \sim 0$ are restricted to a small span across the stream and $|u' - c_{x'}|$ increases in both directions away from these low values. There are two main differences from the previously described float worth noting: First, in this case, the anticipated cat's eye lies to the south of the jet center. (The reader is reminded that critical lines, and thus cat's eyes, appear on both sides of the Gulf Stream due to its nearly symmetric zonal velocity field.) Second, the critical line in this case lies very near the edge of the stream, at approximately the 10 cm s^{-1} isotach, emphasizing that the edge of the jet moves with the critical line and is not fixed to a given isotach.

c. RAFOS 024: Figure 8

RAFOS 024 begins to traverse the stream from south to north near day 337, as reflected in the strong pressure decrease along its path (Fig. 8a). The small downstream velocity also indicates that the float is near the northern edge of the stream. At such a location the float has approached a critical line, as seen by the small difference in u' and $c_{x'}$. The trajectory in the moving frame shows
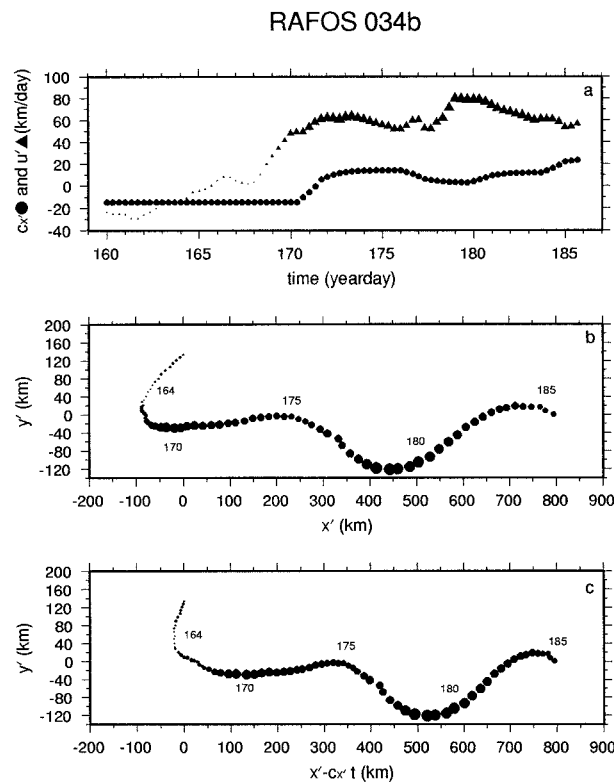
RAFOS 034b

FIG. 9. As for Fig. 4 but for RAFOS 034b.

a cusp at this point, a northern apex (Fig. 8c). This behavior is characteristic of the open trajectories in Fig. 1 that pass close to fixed points; the parcel nears but does not cross a critical line. This contrasts with the second event of interest for this float. On its second approach to the northern edge of the stream, the float approaches a critical line near day 351 and apparently *crosses* the critical line. This change is reflected in the retrograde motion seen for the trajectory in the moving frame. However, unlike RAFOS 037 and RAFOS 035b, this float path does not trace out a cat's eye after it has crossed a critical line. Rather, the float's retrograde motion is short-lived; it quickly returns to its original path south of the critical line. As will be discussed in sections 5 and 6, such behavior is not generally expected in the vicinity of cat's eyes. To explain the uncharacteristically small loop in the vicinity of a critical line we surmise that it results from a small overestimation of the phase speed for this float. A slight reduction in the measured phase speed (within the measurement error) would create a strong cusp at this point rather than the small observed loop.

d. RAFOS 034b: Figure 9

The trajectory for RAFOS 034b illustrates float entrainment. In the early stage of this float record (from days 160 to 164) this float is outside of the jet core, as

evidenced by its westward zonal velocity (Fig. 9a). From the pressure record (Fig. 9a) it is apparent that the float is on the northern edge of the stream. Near day 163 the float approaches the northern critical line from the north, rather than from the south, as for RAFOS 037. When RAFOS 034b crosses the critical line, it apparently begins on a new path, one that is within the stream and progressive, since now $u' > c_{x'}$. From day 167 or 168 the trajectories in the moving and stationary frames do not differ much because $u' > c_{x'}$. For this float only a portion of a cat's eye is evident due to the incompleteness of the record.

5. Mechanism for exchange

Nearly all the trajectories described above indicate fluid exchange between the jet core and the surrounding cat's eye structures. The motion is reminiscent of a fluid particle in the flow field of Fig. 1, which crosses the manifolds separating the regions of open and closed streamlines. As described in section 2, these crossings can occur if perturbations are introduced to the basic state, which consists of a jet with a single, steadily propagating meander. We will refer to the stable and unstable manifolds of the basic state as the undisturbed manifolds, as distinguished from generalized manifolds, which exist in the perturbed flow. The methods of dynamical systems provide insight into how and where fluid particles cross the undisturbed manifolds.

We begin by first examining the generalized manifolds, which occur when the basic flow is disturbed by a perturbation of a different period than that associated with the steadily propagating meander. This flow is no longer steady in the frame moving with the meander phase speed, and a Poincaré section is needed to display information about the trajectories of fluid particles (Fig. 10). The Poincaré section represents a periodic sampling of selected fluid trajectories, with the sampling or "strobing" period T being that of the perturbation (measured in the frame of reference moving with the primary meander). Fixed points appear in the Poincaré section (points p_1 and p_2 in Fig. 10) that correspond to particles with strictly periodic trajectories, with period T. In addition, there are particles whose location at time $t = nT$ approaches the fixed point p_2 as t approaches infinity along the dashed-line curve in the Poincaré section. This curve represents the stable manifold for the fixed point p_2, denoted $W^s(p_2)$, and is a generalization of the stable manifold discussed in section 2 for the undisturbed flow. Other curves map out the locations of fluid particles at time $t = nT$ that approach the fixed point p_1 as t approaches negative infinity (i.e., solid-line curve in Fig. 10), termed the unstable manifold for fixed point p_1, denoted $W^u(p_1)$. Unlike the situation in Fig. 1, the unstable manifold for fixed point p_1 no longer coincides with the stable manifold for p_2. The two curves are distinct and they intersect at an infinite number of points, a few of which are shown. The presence of these in-
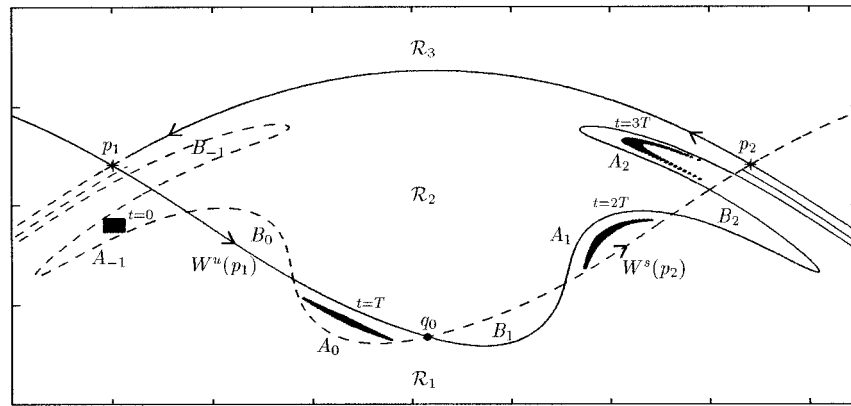
FIG. 10. Schematic of a Poincaré map, from Miller et al. (1997). A portion of the stable manifold for fixed point p_2, $W^s(p_2)$, is identified with the dashed line while a portion of the unstable manifold for the fixed point p_1, $W^u(p_1)$, is indicated by the solid line between region $\mathcal{R}_1$ and $\mathcal{R}_2$. The jet is located in the region $\mathcal{R}_1$, with the fixed points in the vicinity of meander crests.

tersections is a necessary condition for chaotic Lagrangian motion. Between neighboring pairs of intersection points are regions of fluid trapped between the two manifolds (labeled A_i and B_i in Fig. 10), termed "lobes." The fluid in lobe A_{-1} lies to the south of the unstable manifold and to the north of the stable manifold at $t = 0$ and must continue to do so for subsequent time. After a period T, the fluid in A_{-1} moves to lobe A_0 and then to A_1 and so on. In some cases the fluid in lobe A_{-1} will move directly to A_1 and then to A_3, or some other mapping will occur, but flow will always occur in the direction indicated by the arrows on the manifolds. Note that the two manifolds on the northern boundary of the cat's eye will also generally be tangled, although this is not shown in detail in Fig. 10. For a more complete discussion of the lobe mechanism in jets and wakes, readers are referred to Wiggins (1992).

The Poincaré map in Fig. 10 is a tool for anticipating the motion of an individual RAFOS float based on its initial location. If the initial position lies outside of a lobe, which might occur if the float is launched in the jet core or far to the north or south of the jet, the trajectory will be nonchaotic. If the initial position lies within a lobe, for example in A_{-1}, the parcel with be moved from A_{-1} to A_0 to A_1 and so on. In other words, the parcel moves from the outside to the inside of the undisturbed cat's eye, that is, from region R_1 to region R_2. Even if the mapping sequence is different (e.g., A_{-1} to A_1 to A_3), the overall feature of the movement from outside to inside the undisturbed cat's eye persists. Similar comments apply to fluid in lobes B_i moving from region $\mathcal{R}_2$ to $\mathcal{R}_1$. In either case, the crossing of the undisturbed cat's eye boundary may occur over many periods of the primary meander and may therefore be difficult to anticipate using conventional Eulerian representations of the flow field. As fluid enters the undisturbed cat's eye, the associated lobe becomes stretched into a thin filament (e.g., A_2). As time progresses, it

becomes increasingly difficult to anticipate the motion of individual parcels within the lobe. This process is consistent with the chaotic nature of the trajectories near the cat's eye. (A more detailed example of this progression of events is described later.) A dynamical consequence of the filamentation of the lobes is that property gradients are intensified, leading to enhanced erosion by small-scale diffusive processes. To further our analysis of the observed trajectories, lobe structures obtained from a numerical model of a meandering jet (Miller et al. 1997) are presented in section 6 along with numerically simulated fluid particle trajectories.

6. Numerically simulated float trajectories

To augment the analysis of Lagrangian flow fields, techniques from dynamical systems theory are applied to the results from a numerical model of a meandering jet. A theoretical treatment of the chaotic motion of Lagrangian fluid particles from the dynamical systems approach has traditionally been restricted to kinematic descriptions of flows that are periodic (or quasi-periodic) and conservative. The numerically simulated meandering jet flow presented below has two dominant timescales (one associated with the propagation speed of the meanders and one associated with a pulsation in meander amplitude), but is not strictly quasi-periodic, nor is it conservative. Recently, however, stable and unstable manifolds for the numerically simulated flow have been constructed from the model data (Miller et al. 1997). As discussed in section 5, the manifolds provide a framework in which the chaotic motion of Lagrangian particles can be described through the process of "lobe dynamics." We will illustrate this process in the numerical model and examine the trajectories of four Lagrangian fluid particles that exhibit characteristics similar to the RAFOS float trajectories presented in section 4.
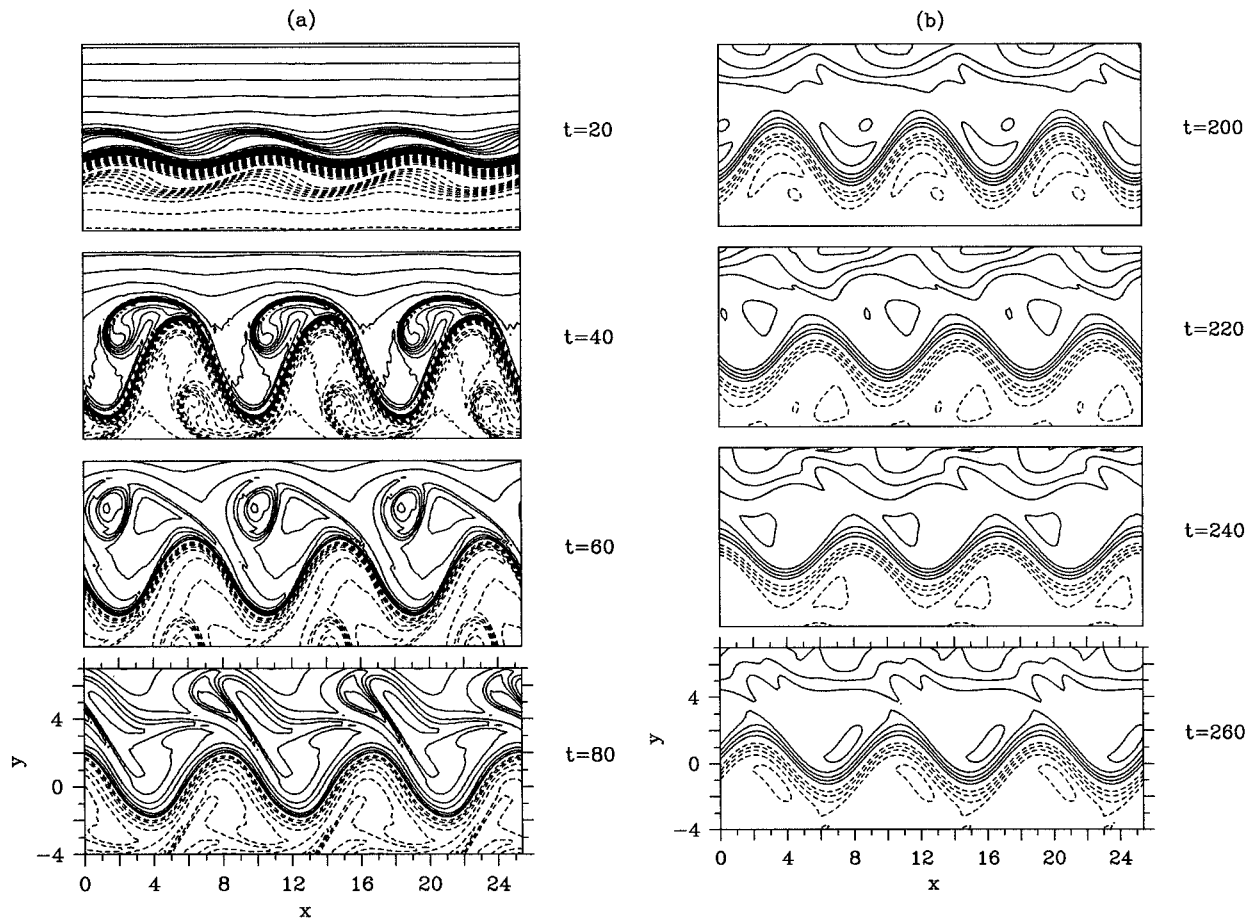
FIG. 11. Nonlinear evolution of the weakly perturbed flow into a meandering jet, represented in terms of the potential vorticity field. Note that only a portion of the computational domain in the meridional direction is illustrated. (a) Early nonlinear development, $t = 20, 40, 60,$ and 80. (b) The nearly quasiperiodic, quasi-steady regime, $t = 200, 220, 240,$ and 260. The contour increment is $\Delta q = 0.1$.

The meandering jet flow is simulated numerically using the pseudospectral model of Flierl et al. (1987) for the nondimensional, barotropic, beta-plane equations:

$$\nabla^2\psi_t + J(\psi, \nabla^2\psi) + \beta\psi_x = (1/R_e)\nabla^4\psi. \qquad (2)$$

Our formulation differs only slightly from Flierl et al. (1987) in that we use Newtonian viscosity instead of superviscosity, and we control the numerical amplification of high modes by applying a weak exponential cut-off filter to the pseudospectral approximation of the potential vorticity, $q = \nabla^2\psi + \beta y$. The computation of Lagrangian fluid trajectories, given by

$$d\mathbf{X}/dt = \mathbf{u}(\mathbf{x} = \mathbf{X}(t), t), \qquad (3)$$

is performed using a fourth-order Adams predictor–corrector to update the particle positions and a sixth-order Lagrange interpolation to estimate the local flow velocity at off-grid points. The results presented here correspond to simulations with nondimensional $\beta = 0.103$ and Reynolds number $\text{Re} = 10^3$, with numerical quantities approximated using 128 Fourier modes on a square computational domain of nondimensional length 25.6.

The spatial resolution is sufficient to ensure that the viscous dissipation in the flow dominates the numerical dissipation. We associate the nondimensional value $\beta = 0.103$ with dimensional $\beta^* = 1.8 \times 10^{-11}$ m^{-1} s^{-1} $= \beta U^*/L^{*2}$, where $U^* = 175$ cm s^{-1} and $L^* = 100$ km. The corresponding eddy viscosity is $U^*L^*/\text{Re} = 175$ m^2 s^{-1}. Following Flierl et al. (1987), we chose $\beta = 0.103$ as representative of the Gulf Stream.

The numerical investigation presented here is intended to be used for qualitative comparison with the RAFOS float trajectory data, providing a basis of understanding for the pathways taken by the selected RAFOS floats. There are some obvious differences between the barotropic model and the Gulf Stream flow field; however, for our purpose here these differences are generally unimportant. In a comparison of Lagrangian pathways it is important that the numerical flow field is dynamically consistent, exhibits a dominant meandering mode, and has a secondary temporal periodicity. These few characteristics lead to generic Lagrangian behavior exhibited in both the model and the Gulf Stream trajectories, as will be shown.
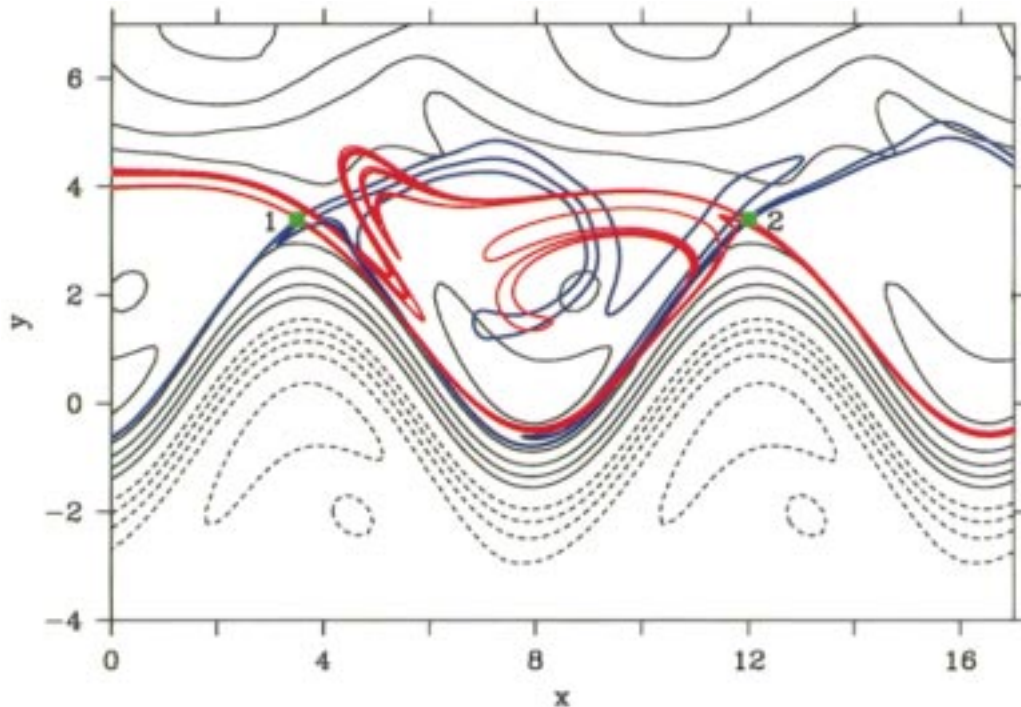
FIG. 12. Potential vorticity contours over a portion of the domain at time $t = t_0 = 200$. Two fixed points for the flow are indicated in green. Portions of the stable and unstable manifolds (from Rogerson et al. 1997) for the flow are shown in blue and red, respectively. The contour increment for the potential vorticity is $\Delta q = 0.1$.

In the numerically simulated flow, a weakly perturbed zonal jet evolves nonlinearly into a large-amplitude meandering configuration, as shown in Fig. 11a for the potential vorticity field. Later, the flow saturates to an approximately quasiperiodic, quasi-steady state characterized by a zonally propagating meandering jet with pulsating meander amplitude (Fig. 11b). It is this late-stage regime that is the focus of our analysis. We have arbitrarily selected $t = t_0 = 200$ (first frame in Fig. 11b) as the initial time for the numerical experiments. In the discussion that follows, we apply the term ''jet core'' to the region represented by the open potential vorticity contours meandering between $y \sim \pm 3$.

The analysis of Miller et al. (1997) has identified hyperbolic fixed points in this numerical flow field and has calculated stable and unstable manifolds associated with those points. In Fig. 12, contours of potential vorticity over a portion of the computational domain are shown, and two fixed points on the northern side of the jet are indicated, fixed point 1 located near $(x, y) = (3.5, 3.4)$ and fixed point 2 located near $(x, y) = (12.0, 3.4)$. Superimposed on the potential vorticity field in Fig. 12 are portions of the stable and unstable manifolds (shown in blue and red, respectively) for fixed points 1 and 2. As mentioned in section 5, the fact that the curves representing the stable and unstable manifolds are distinct and intersect, or ''tangle,'' is a necessary condition for chaotic Lagrangian motion. These intersections create more prominent lobes in the northern portion of the

(untangled) cat's eye and result in thin, elongated lobes in the southern portion of the cat's eye near the edge of the jet core.

As described in section 5, the lobes created by the intersections of the stable and unstable manifolds define the motion of fluid particles from one lobe to another. Since the lobes for the numerical flow in Fig. 12 are more complicated than those depicted in Fig. 10, we have isolated one set of lobes for illustration in Fig. 13. In the numerically simulated flow, fluid that lies inside lobe L1 (outlined in blue) at time $t = t_0$ is advected to lobe L2 (outlined in green) at time $t = t_0 + T$, and then to lobe L3 (outlined in red) at time $t = t_0 + 2T$, where T is the pulsation period in the meander amplitude. That lobe L3 is extremely thin makes it difficult to make a determination about the fate of individual Lagrangian particles, but its configuration does suggest that some fluid elements will be located along the edge of the jet core at $t = t_0 + 2T$, while others will be located away from the jet core. Since portions of lobes L2 and L3 are near the edge of the jet core, particles outside the jet in L1 may have the opportunity to become entrained into the jet. The initial location of one such particle is indicated by the triangle in Fig. 13, and its numerical trajectory will be presented below. The movement of this particle from lobe L1 to lobe L2 and L3 is illustrated in Fig. 14.

Similarly, the location and geometry of the lobes can be used to anticipate the detrainment of particles from
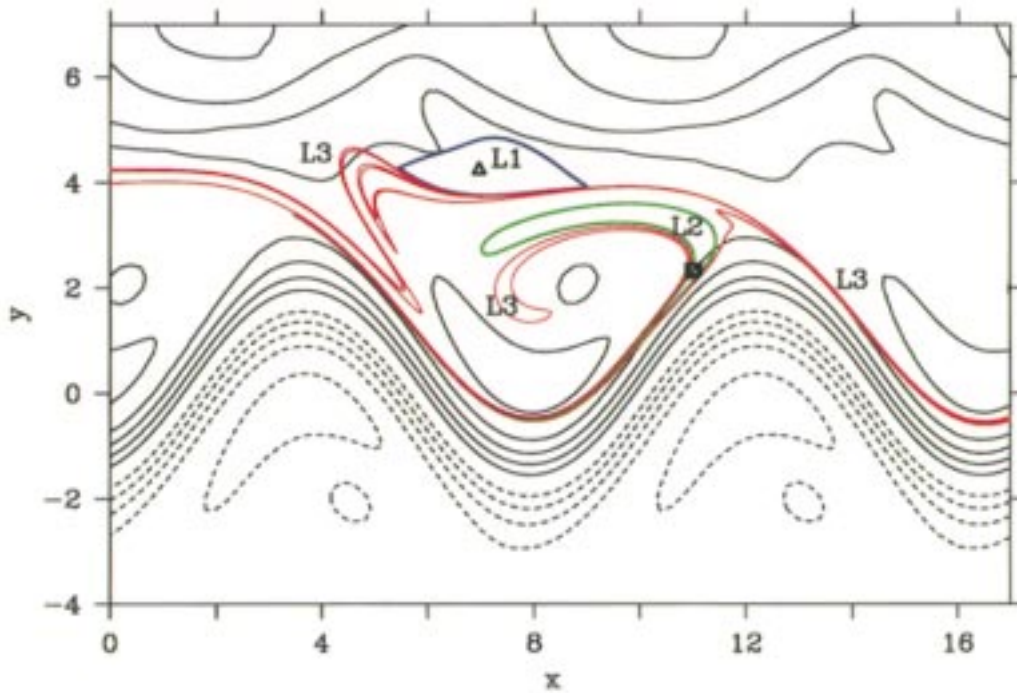
FIG. 13. Potential vorticity contours at time $t = t_0 = 200$ and a set of lobes. We refer to the lobe outlined in blue as L1 and associate it with time $t = t_0$. L1 is mapped to the green lobe, L2, one period later at time $t = t_0 + T$. The L3 lobe, outlined in red, corresponds to time $t = t_0 + 2T$. The four representative numerical Lagrangian trajectories presented in the text have initial positions indicated by the squares (three particles) and by the triangle.
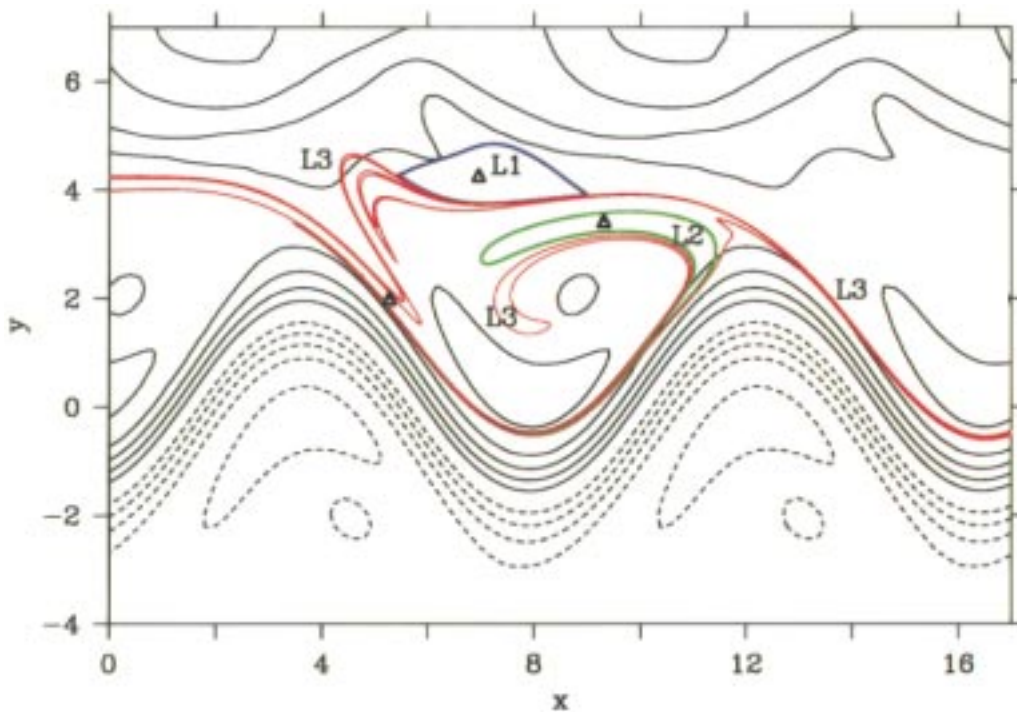

FIG. 14. The movement of a representative particle, represented by the triangle, from L1 (outlined in blue) to L2 (in green) and L3 (in red). The location of the particle has been translated to a reference frame moving with the phase speed of the meanders and mapped possibly multiple wavelengths to collocate its position with the lobes computed for the fixed points indicated in Fig. 11.
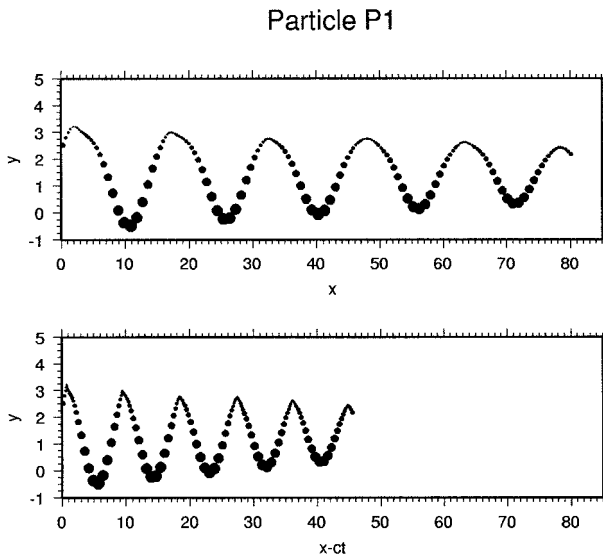
Particle P1

Particle P2

FIG. 15. Trajectory for numerical particle P1 with initial position indicated by the square in Fig. 12. The initial position has been shifted for illustration to $X(t = t_0) = 0$ and the size of the marker scaled with the magnitude of $u - c_x$. (a) Trajectory in the stationary reference frame. (b) Trajectory in the moving reference frame.

FIG. 16. As for Fig. 15 but for numerical particle P2.

the jet. In the southern part of the cat's eye near the northern edge of the jet core, the manifolds (for the finite portions shown) appear to only intersect the jet core on the leading edge of the crest (Fig. 12). Lobe L2 is one that intersects the jet core (green lobe in Fig. 13), and therefore we might expect that a particle could leave the jet by moving from lobe L2 to lobe L3. That is, jet fluid in this part of lobe L2 could get transported to the section of lobe L3 (red lobe in Fig. 13) that is outside the jet. This detrainment process is demonstrated by considering the numerical trajectories of three fluid particles with initial positions indicated by the squares in Fig. 13, each within 0.05 nondimensional units of each other. We will refer to these particles as P1, P2, and P3. In addition, because the particles are within the lobe structure of the flow, we can expect the motion to be chaotic and the fate of the three particles to be different.

The trajectory for fluid particle P1 is shown in Fig. 15. Particle P1 travels along the northern edge of the jet core for the duration of the simulation. As the particle periodically moves through the meander crests, it approaches the critical line where $u - c = 0$ but fails to cross it. In the moving reference frame, the particle's motion near the critical line results in cusps in its trajectory. The cusplike characteristics of this particle trajectory can be compared with the path of RAFOS 024. Figure 16 shows the trajectory for particle P2. For the first two periods, from time $t = t_0$ to $t = t_0 + 2T$, the trajectory of particle P2 is similar to that of P1. Particle P2, however, does cross a critical line. The trajectory in the stationary reference frame exhibits loops near the crests of the jet core. While it appears in the stationary frame that the particle continues along the edge of the

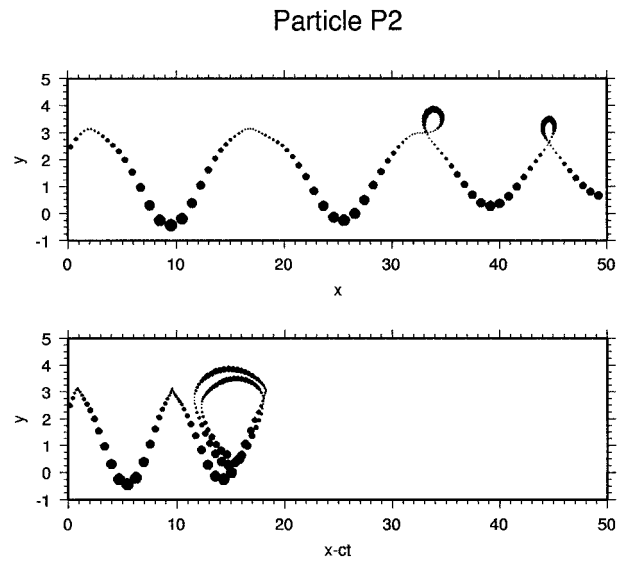jet core after making the looping excursions near the crests, we can see from the trajectory in the moving reference frame that this looping pathway is indicative of the particle's movement in the cat's eye. Although the data is limited, the trajectories of RAFOS 037 and 035b suggest the same looping pattern, indicating that toward the end of their missions the floats may have begun to move within the cat's eye region on the northern (037) and southern (035b) side of the stream.

Figure 17 shows the trajectory for the last of three particles, P3, initialized at the position indicated by the square in Fig. 13. Again, for the first two periods the path of particle P3 is similar to that of P1 and P2. Particle P3 also crosses a critical line and leaves the edge
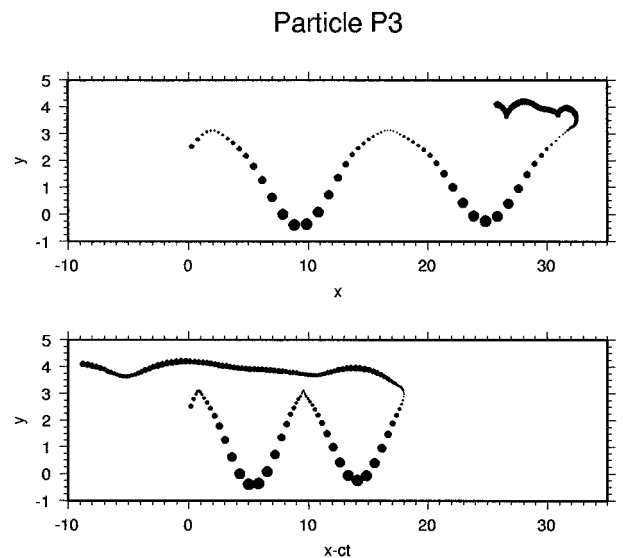
Particle P3

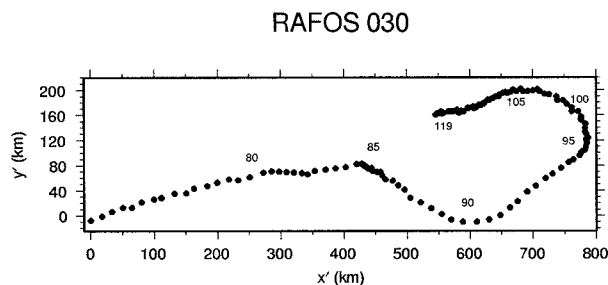FIG. 17. As for Fig. 15 but for numerical particle P3.

RAFOS 030

FIG. 18. Stationary frame trajectory for RAFOS 030. The along-stream axis for this trajectory is aligned with the mean Gulf Stream path, at approximately 16° to the horizontal.

Particle P4

Fig. 19. As for Fig. 15 but for numerical particle P4 whose initial position is indicated by the triangle in Fig. 12.

of the jet core. However, rather than escaping from the jet core to a cat's eye, when the particle leaves the jet core it travels north of the cat's eye and into a region of retrograde flow, as its trajectory clearly indicates. Although such retrograde motion was not evident in any of the 11 RAFOS trajectories used in this study, such behavior is observed in the larger set of RAFOS float trajectories. An example is provided by the trajectory for RAFOS 030, shown in the stationary frame in Fig. 18. Although there is no phase speed data available for this float, it is evident from its path (and also its associated pressure record, not shown) that this float leaves the core of the Gulf Stream and moves westward north of the stream [presumably as part of the mean westward recirculation north of the Gulf Stream (Hogg et al., 1986)]. Using pressure and velocity records as indicators, the float is determined to be "out" of the stream for ~30 days. Given that this temporal period approximately matches a Gulf Stream meander period, and that the float shows no sign of periodicity in its path, it is assumed that this float has moved from the jet core to the region north of the stream, outside of the cat's eye in the moving frame. Both the numerical and observational trajectories serve as evidence that escape from the jet core can be to either a cat's eye or to the region outside of the cat's eye.

Last, we consider a particle, P4, with initial position outside the jet at the location indicated by the triangle in Fig. 13. This particle is entrained into the jet by the L1-to-L2-to-L3 lobe process described above. As shown in Fig. 19, the particle initially travels westward, then enters the circulating region in the cat's eye, before becoming entrained into the jet core. Apart from the excursion around the cat's eye region, the trajectory of particle P4 can be compared favorably with the trajectory of RAFOS 034b.

7. Summary

A major contribution of this work is that RAFOS float trajectories have been placed in a moving frame of reference for the first time. When float trajectories are viewed in a frame moving with the primary m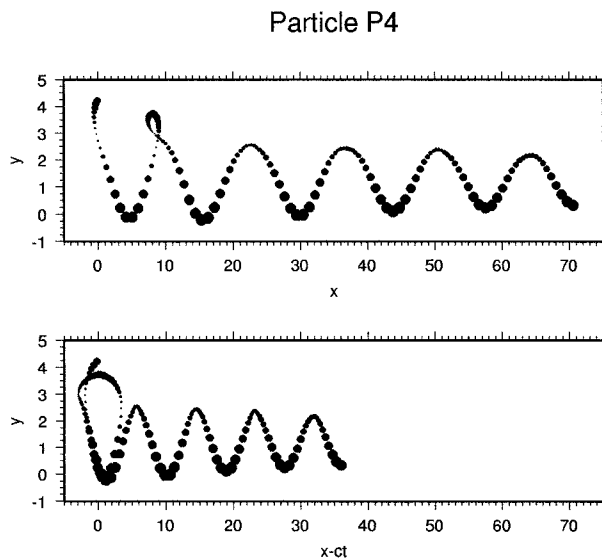eander phase speed, geometrical structures emerge that allow for new interpretations of the data. The presence of looping and oscillatory behavior in the same trajectory suggests that the float is crossing in and out of cat's eyes structures, either from within the jet core or from outside of the jet. In doing so, the float tends to cross the critical line defined using the primary meander phase speed. Crossings are associated with lobes of fluid that move in and out of the cat's eyes. Since lobes typically become filamented and vulnerable to small-scale processes, we interpret the float crossings as an indication of mixing, which will effect any property that possesses a mesoscale gradient.

The analysis presented in sections 5 and 6 shows how chaotic exchange can result solely from the jet's temporal variability. This is not to say that external factors, such as rings colliding with the stream, do not contribute to fluid exchange between the Gulf Stream and the surrounding waters. Rather, our work here demonstrates that the fundamental mechanics of a temporally varying jet produces lobes of fluid that are entrained and detrained from the edge of the jet, producing chaotic exchange. Interestingly, the geometry of the lobes is suggestive of the filaments that have frequently been observed "trailing" from Gulf Stream meander crests and troughs. The lobes shown in this paper and the observed filaments display a gradual thinning as the volume of fluid is drawn from the jet. Should property gradients exist within the lobes, the filamentation process amplifies the gradients, rendering the properties more vulnerable to diffusive mixing.

The general characterization of RAFOS float behavior in a moving frame of reference matches well with the characterizations drawn from an analysis of trajectories simulated from a barotropic numerical model. This match is made despite the obvious differences in the
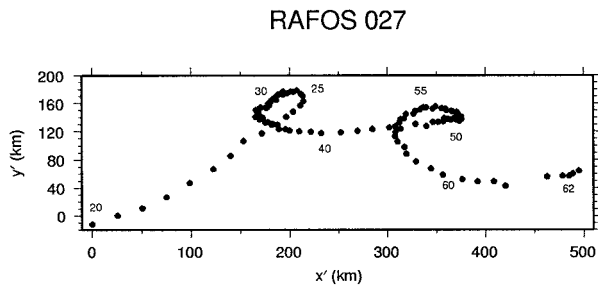
RAFOS 027

FIG. 20. Stationary frame trajectory for RAFOS 027. The along-stream axis for this trajectory is aligned with the mean Gulf Stream path, at approximately 16° to the horizontal.

dynamical structure of the observed and numerical fields, namely in terms of the background potential vorticity gradient. Across the Gulf Stream, at the depth of the RAFOS float trajectories studied in this paper, there is a weak potential vorticity gradient that does not inhibit the crossing of floats from one side of the stream to the other, as detailed by Bower and Lozier (1994). In the numerical jet discussed in section 5 there is a strong potential vorticity gradient across the center of the jet that acts as an effective barrier to fluid exchange across the jet. Because our concern here is with fluid exchange between the jet and the region outside of the jet, our results are somewhat insensitive to the differences in the potential vorticity gradient that characterizes the center of the jet. The similarities observed in the two sets of trajectories does not stem from strict similarity in dynamics but, rather, is a result of the kinematic similarities in their flow fields. Basically, the flow structures, and hence trajectory features, rely on the presence of a critical line(s) in the flow field. This critical line, in turn, depends primarily on the zonal velocity of the flow and the phase speed of the meander. A secondary periodicity is crucial to the development of exchange, but its nature or strength is not generally important. That the two sets of trajectories have such similar features confirms that the exchange of floats in and out of the Gulf Stream is generally dictated by the periodicity of the jet.

From viewing the trajectories in a moving fame of reference the interpretation of trajectories in a stationary frame has also benefited. In other words, it is now possible to recognize features in the stationary frame and interpret those features in terms of cat's eyes and critical lines. For instance, RAFOS 027, shown in Fig. 20, does not have any associated phase data, so our only choice is to view the trajectory in its stationary frame. The pattern of this float is clearly similar to the pattern displayed by P2 (Fig. 16). Based on this similarity, we would now interpret the small loops in RAFOS 027's path as evidence that the float has been entrained in a cat's eye and is circulating within that cell.

Finally, it is clear from this work that we have been working with a float dataset that was not suited for the purpose of studying exchange processes. Indeed, the

RAFOS floats were embedded within the center of the stream to maximize their residence time in the stream. It is suggested that to better understand the dynamics associated with the fluid and property exchange between oceanic jets and their surrounding waters, float deployment be made at and near the vicinity of the jet's edge to detail the mechanisms of entrainment and detrainment. As illustrated with this work, to maximize the utility of float data, it should be accompanied by phase speed information to allow for moving frame of reference analyses.

REFERENCES

Behringer, R. P., S. D. Meyers, and H. L. Swinney, 1991: Chaos and mixing in a geostrophic flow. *Phys. Fluids A,* **3,** 1243–1249.

Bower, A. S., 1991: A simple kinematic mechanism for mixing fluid parcels across a meandering jet. *J. Phys. Oceanogr.,* **21,** 173–180.

——, and T. Rossby, 1989: Evidence of cross-frontal exchange processes in the Gulf Stream based on isopycnal RAFOS float data. *J. Phys. Oceanogr.,* **19,** 1177–1190.

——, and M. S. Lozier, 1994: A closer look at particle exchange across the Gulf Stream. *J. Phys. Oceanogr.,* **24,** 1399–1418.

——, T. Rossby, and R. O'Gara, 1986: RAFOS Float Pilot Studies in the Gulf Stream. University of Rhode Island Tech. Rep. 86-7, 110 pp. [Available from Graduate School of Oceanography, University of Rhode Island, Narragansett, RI 02882.]

Cornillon, P., T. Lee, and G. Fall, 1994: On the probability that a Gulf Stream meander crest detaches to form a warm core ring. *J. Phys. Oceanogr.,* **24,** 159–171.

del-Castillo-Negrete, D., and P. J. Morrison, 1993: Chaotic transport by Rossby waves in shear flow. *Phys. Fluids A,* **5,** 948–965.

Duan, J., and S. Wiggins, 1996: Fluid exchange across a meandering jet with quasiperiodic variability. *J. Phys. Oceanogr.,* **26,** 1176–1188.

Dutkiewicz, S., A. Griffa, and D. B. Olson, 1993: Particle diffusion in a meandering jet. *J. Geophys. Res.,* **98,** 16 487–16 500.

Flierl, G. R., P. Malanotte-Rizzoli, and N. J. Zabusky, 1987: Nonlinear waves and coherent structures in barotropic β-plane jets. *J. Phys. Oceanogr.,* **17,** 1408–1438.

Gangopadhyay, A., 1990: Wind forcing of the Gulf Stream: A space–time analysis. Ph.D. Dissertation, University of Rhode Island, 190 pp. [Available from Graduate School of Oceanography, University of Rhode Island, Narragansett, RI 02882.]

Hogg, N. G., R. S. Pickart, R. M. Hendry, and W. J. Smethie Jr., 1986: The northern recirculation gyre of the Gulf Stream. *Deep-Sea Res.,* **33,** 1139–1165.

Lee, T., 1994: Variability of the Gulf Stream path observed from satellite infrared images. Ph.D. Dissertation, Graduate School of Oceanography, University of Rhode Island, 188 pp. [Available from Graduate School of Oceanography, University of Rhode Island, Narragansett, RI 02882.]

——, and P. Cornillon, 1995: Temporal variation of meandering in-

tensity and domain-wide lateral oscillations of the Gulf Stream. *J. Geophys. Res.,* **100,** 13 603–13 613.

——, and ——, 1996a: Propagation of Gulf Stream meanders between 74° and 70°W. *J. Phys. Oceanogr.,* **26,** 205–224.

——, and ——, 1996b: Propagation and growth of Gulf Stream meanders between 75° and 45°W. *J. Phys. Oceanogr.,* **26,** 225–241.

Lozier, M. S., and D. Bercovici, 1992: Particle exchange in an unstable jet. *J. Phys. Oceanogr.,* **22,** 1506–1516.

——, T. J. Bold, and A. S. Bower, 1996: The influence of propagating waves on cross-stream excursions. *J. Phys. Oceanogr.,* **26,** 1915–1923.

Meyers, S. D., 1994: Cross-frontal mixing in a meandering jet. *J. Phys. Oceanogr.,* **24,** 1641–1646.

Miller, P. D., C. K. R. T. Jones, A. M. Rogerson, and L. J. Pratt, 1997: Quantifying transport in numerically generated vector fields. *Physica D,* in press.

Pierrehumbert, R. T., 1991: Chaotic mixing of tracer and vorticity by modulated travelling Rossby waves. *Geophys. Astrophys. Fluid Dyn.,* **58,** 285–319.

Pratt, L. J., M. S. Lozier, and N. Beliakova, 1995: Parcel trajectories in quasigeostrophic jets: Neutral modes. *J. Phys. Oceanogr.,* **25,** 1451–1466.

Samelson, R. M., 1992: Fluid exchange across a meandering jet. *J. Phys. Oceanogr.,* **22,** 431–440.

Song, T., T. Rossby, and E. Carter, 1995: Lagrangian studies of fluid exchange between the Gulf Stream and surrounding waters. *J. Phys. Oceanogr.,* **25,** 46–63.

Wiggins, S., 1992: *Chaotic Transport in Dynamical Systems.* Springer-Verlag, 301 pp.